BMC Cancer

RESEARCH

Open Access

E2F2(E2F transcription factor 2) as a potential therapeutic target in meibomian gland carcinoma: evidence from functional and epigenetic studies

Wei Wang[1†], Hetong Wang[1†], Xun Liu[1], Fei Xu[2], Qin Tang[3], Chuanli Zhang[4], Jiaqi Lin[5], Limin Zhu[1*] and Tingting Lin[1*]

Abstract

Background Meibomian Gland Carcinoma (MGC) is a highly malignant eyelid tumor with a poor prognosis. This study investigates the molecular mechanisms underlying MGC, focusing on the abnormal expression of E2F transcription factor 2 (E2F2), often observed in tumors and potentially linked to DNA methylation.

Methods E2F2 expression was measured in MGC cells and tissues. Tissue samples from 3 normal meibomian glands (MG) and 36 MGC patients were used to construct a tissue microarray. Functional assays were performed by modifying E2F2 expression, including CCK8, wound healing, Transwell, and analysis of epithelial-mesenchymal transition (EMT)-related markers. Flow cytometry was used to assess cell apoptosis and cell cycle. RNA sequencing was conducted to identify differential genes after treating MGC cells with the methylation inhibitor 5-aza-2′-deoxycytidine (5-aza-2-dc), to explore the relationship between E2F2 downregulation in MGC and methylation.

Results E2F2 expression was significantly lower in MGC cells compared to normal MG cells. Immunohistochemical analysis showed low E2F2 expression in MGC. Specifically, immunohistochemical staining results have revealed a negative correlation trend between E2F2 and Ki-67 expression, as well as a positive correlation trend between E2F2 and P21, P27 expression. E2F2 knockdown increased MGC cell proliferation, migration, and invasion. Flow cytometry revealed that E2F2 knockdown reduced apoptosis, decreased the G0/G1 phase, and increased the S phase, while E2F2 overexpression produced opposite effects. RNA sequencing revealed that a total of 87 genes were differentially expressed in the 5-aza-2-dc experimental group compared to the control group, with 72 mRNAs showing upregulated expression and 15 mRNAs showing downregulated expression. Bioinformatics analysis results indicated that the functions of these differentially expressed genes were concentrated, and the biological processes mainly involved DNA replication, among others. The signaling pathways associated with these genes primarily included DNA replication and the cell cycle. RNA sequencing identified differential gene expression after methylation inhibition in MGC cells with 5-aza-2-dc, demonstrating that demethylation significantly upregulated E2F2. MSP assays

[†]Wei Wang and Hetong Wang made the equal contributions to the article.

*Correspondence:
Limin Zhu
zlmjojo@163.com
Tingting Lin
ltt6123@126.com
Full list of author information is available at the end of the article

confirmed reduced methylation levels. Additionally, inhibiting gene methylation in MGC cells suppressed proliferation, migration, and invasion.

Conclusion E2F2 presents a promising therapeutic target for MGC. Overexpression of E2F2 and methylation inhibition in MGC cells may reverse E2F2 gene silencing, inhibiting malignant progression. These findings provide new perspectives for targeted therapies and precise, individualized treatment in MGC.

Keywords Meibomian Gland Carcinoma, E2F2, Cell Cycle, 5-aza-2′-deoxycytidine, RNA Sequencing DNA Methylation

Background

Meibomian gland carcinoma (MGC) is a malignant tumor originating in the meibomian glands within the eyelid and is the second most common type of eyelid malignancy [1]. MGC is characterized by its local aggressiveness and potential for metastasis to regional lymph nodes and distant organs [2, 3]. Its early clinical presentation often mimics benign eyelid lesions, leading to frequent misdiagnosis or delayed diagnosis, which can result in missed opportunities for optimal intervention. Thus, early detection and a comprehensive treatment approach are crucial for enhancing patient outcomes [4]. The current standard treatment for MGC involves surgical excision with regional lymph node dissection [5]. Targeted therapies that inhibit specific proteins or signaling pathways involved in tumor progression aim to prevent DNA damage in cancer cells [6, 7]. However, the pathogenesis of MGC remains poorly understood, highlighting the need to identify effective molecular targets to improve cure rates and reduce mortality.

E2F transcription factor 2 (E2F2) significantly regulates the cell cycle, differentiation, and apoptosis [8]. Abnormal expression of E2F2 is often associated with tumor development, metastasis, and recurrence [9–12]. Dysregulation of E2F2 during carcinogenesis may result from alterations in upstream regulatory elements or epigenetic modifications [13]. Studies have shown that aberrant expression of E2F2 in tumorigenesis and cancer progression is associated with DNA methylation, specifically, particularly CpG methylation, which serves as a regulatory mechanism for E2F activity [14]. During developmental processes, E2F2 has essential regulatory functions through its interaction with SIX1, specifically in methylation [15]. In clear cell renal carcinoma, E2F2 is regarded as a potential target for immunotherapy, influenced by DNA methylation [16].

The development and progression of MGC are influenced by genetic and epigenetic factors, with DNA methylation as a key epigenetic mechanism [17]. DNA methylation is characterized by the covalent attachment of a methyl group to the 5th carbon of cytosine residues in CpG dinucleotides, a process mediated by DNA methyltransferases. This modification regulates gene expression without altering the DNA sequence, typically reducing transcriptional activity and resulting in heritable phenotypic changes. The DNA methyltransferase inhibitor 5-aza-2′-deoxycytidine (5-aza-2-dc) effectively inhibits these enzymes, decreases DNA methylation levels, reverses gene methylation, and restores gene expression [18]. However, the connection between E2F2 expression and DNA methylation in MGC remains unclear.

This study aims to investigate the role and molecular mechanisms of E2F2 in MGC to evaluate its potential as a biomarker and therapeutic target. The results are anticipated to offer fresh theoretical perspectives for the clinical management of MGC.

Materials and methods

Materials

The following reagents were used in this study: RPMI-1640 medium (Gibco, USA), phosphate-buffered saline (PBS) (Gibco, USA), fetal bovine serum (FBS) (Gibco, USA), penicillin–streptomycin (HyClone, USA), TRIzol reagent (Ambion, USA), 5-aza-2-dc (Sigma-Aldrich, USA), a DNA extraction kit (EZBioscience, USA), an apoptosis detection kit (KeyGEN BioTECH, China), a cell cycle analysis kit (KeyGEN BioTECH, China), E2F2(1:750, Affnity, China, AF4100), GAPDH(1:10,000, Affnity, China, AF7021), P21(1:100, Affnity, China, AF3290), P27(1:100, Affnity, China, DF6090), Ki-67(1:100, Affnity, China, AF0198), β-tubulin(1:3000, Affnity, China, AF7011), β-actin(1:8000, Affnity, China, AF7018), E-cadherin(1:2000, Affnity, China, AF0131), Bax(1:1000, Affnity, China, AF0120), Caspase3(1:1000, Affnity, China, AF7022), Goat Anti-Rabbit IgG(H + L) HRP(1:7000, Affnity, China, S0001). Formalin- and paraffin-embedded specimens were collected from Tianjin University Eye Hospital.

Analysis of E2F2 expression differences in various tumor tissues using public databases

The "Gene DE" module in the TIMER2.0 (Tumor Immune Estimation Resource, version 2) public database was utilized to analyze the expression differences of E2F2 between various tumor tissues and their

adjacent normal tissues. By entering the gene "E2F2," data were retrieved to assess its expression levels across multiple tumor types.

Primary cell culture

Three primary MGC cells (M1, M2, M3) were isolated from newly diagnosed patients without prior radiotherapy or chemotherapy. Following preliminary diagnosis, patients underwent Mohs micrographic surgery, and portions of the excised tumor tissue and adjacent MG tissue were used for primary cell culture. Postoperative histopathological examination confirmed MGC in the tumor tissues, while adjacent MG tissues were identified as normal, showing no cancer cell infiltration. Tissue specimens were washed with D-Hanks buffer (Meilunbio, China) to remove blood and debris, then cut into approximately 1 mm^3 pieces using a sterile scalpel. These tissue fragments were gently placed into culture flasks containing 10% FBS and 1% penicillin/streptomycin in complete medium (Gibco, USA) and were incubated in a 5% CO_2 incubator at 37 °C (Thermo Fisher Scientific, USA). After cell migration began, the medium was refreshed every two days. Once cells reached approximately 90% confluence, they were passaged using trypsin. After 3–4 passages, relatively pure MGC and MG cells were obtained [19]. Cells from the 4th to 10th passages were used for subsequent experiments in the logarithmic growth phase.

RNA extraction and real-time quantitative polymerase chain reaction (RT-qPCR)

Total RNA was isolated utilizing an RNA extraction kit (EZBioscience, USA), and its concentration was measured. The RNA was then converted into complementary DNA (cDNA) utilizing a reverse transcription kit (EZBioscience, USA). Fluorescent RT-qPCR amplification was performed utilizing the 2×Color SYBR Green qPCR Master Mix kit (EZBioscience, USA). The PCR protocol included a preheating step at 95 °C for 5 min, followed by 40 cycles of 10 s at 95 °C and 30 s at 60 °C. Relative mRNA expression levels were calculated utilizing the $2^{-\Delta\Delta CT}$ method, with GAPDH as the internal control gene. The primer sequences used are listed in Table 1.

Western blot analysis

Total proteins were isolated from cells utilizing a total protein extraction kit (Solarbio, China), with the addition of lysis buffer. Protein level was determined utilizing a BCA protein assay kit (Solarbio, China), followed by denaturation of the proteins through heating at 99 °C for 10 min. The denatured proteins were isolated utilizing SDS-PAGE electrophoresis and then transferred onto a PVDF membrane. The membrane was treated with 5% bovine serum albumin (BSA) (ZSGB-BIO, China) to block nonspecific binding at RT for 2 h, followed by incubation with primary antibodies overnight at 4 °C. The membrane was then washed with TBST (Solarbio, China) and incubated with secondary antibodies for 2 h at RT. After additional washes with TBST, protein bands

Table 1 Primer Sequences

Gene Name	Forward(5′→3′)	Reverse(5′→3′)
ESM1	ACCTTCGGGATGGATTGCAG	CCGGGATCAGCGTGGATTTA
OPCML	GGGTTCACCTAATAGTGCAAGTT	CATCCTCACTTACAAAGCCCTG
E2F2	CTGAAGGAGCTGATGAACACG	CCCTTGGGTGCTCTTGAGATA
FAM111B	GCCCTTGAAATGCAGAATCCA	GCTGTAAACACACTACGGTCTAA
MCM10	CCCCTACAGACGATTTCTCGG	CAGATGGGTTGAGTCGTTTCC
CLSPN	TGGAGAGTGGGGTCCATTCAT	CCGGGGTTTACGTTTGAAGAAA
MT2A	CCCGCTCCCAGATGTAAAGA	ATAGCAAACGGTCACGGTCAG
CDC45	CTTGAAGTTCCCGCCTATGAAG	GCATGGTTTGCTCCACTATCTC
CDC6	CCAGGCACAGGCTACAATCAG	AACAGGTTACGGTTTGGACATT
EXO1	TGAGGAAGTATAAAGGGCAGGT	TGTGATATTGATAGACCGGGTGA
E-cadherin	TGGACCGAGAGAGTTTCCCT	CAAAATCCAAGCCCGTGGTG
BAX	CCCGAGAGGTCTTTTTCCGAG	CCAGCCCATGATGGTTCTGAT
CASPASE3	AGAGGGGATCGTTGTAGAAGTC	ACAGTCCAGTTCTGTACCACG
P16	GCCCAACGCACCGAATAGTT	ATGGTTACTGCCTCTGGTGC
P21	TGCCGAAGTCAGTTCCTTGT	CATTAGCGCATCACAGTCGC
P27	TCGGACAGTGATCCACCCTA	GGTTCCCTTCGCCAATCACT
CDK4	GTCTATGGTCGGGCCCTCT	CCATAGGCACCGACACCAAT
GAPDH	GATGCTGGCGCTGAGTACG	GCTAAGCAGTTGGTGGTGC

were detected utilizing an ECL detection reagent, and chemiluminescent signals were captured with an imaging analyzer. Quantitative analysis was conducted utilizing ImageJ software.

Hematoxylin and Eosin (HE) and immunohistochemical (IHC) staining

Tissue samples from 3 normal MG and 36 MGC patients were collected to construct a tissue microarray. Tissue specimens were fixed, dehydrated, embedded in paraffin, and sectioned at 3 μm. For HE staining, sections were stained with hematoxylin and eosin (Solarbio, USA), dehydrated, cleared, and mounted. For IHC staining, sections underwent antigen retrieval, blocking, and incubation with primary antibodies at 4 °C overnight. They were then treated with a secondary antibody, developed with DAB, counterstained with hematoxylin, dehydrated, cleared, and mounted. Images were captured using an OLYMPUS inverted light microscope (Japan).

Cell transfection and lentiviral overexpression

The cells were cultured in 6-well plates until they reached 60%–80% confluency. For transfection, 250 μl of Opti-MEM reduced-serum medium (Yuanpei, China) was utilized to dilute the siRNA (Heyuan Bioscience, China), and another 250 μl of Opti-MEM was employed to dilute 5 μl of Lipofectamine 3000 (Invitrogen, USA). Both solutions were incubated separately at RT for 5 min. The diluted siRNA and Lipofectamine 3000 were combined and allowed to incubate for another 20 min at RT (500 μl per well) and were introduced into the cells and mixed gently. The siRNA sequences used in the experiment are listed in Table 2.After 6 h of incubation, the medium was replaced with a fresh culture medium. MGC cells were divided into two groups: a negative control group labeled NC^{SI} and an experimental group labeled $E2F2^{SI}$. The collection times for cell samples after small interfering RNA (siRNA) treatment are as follows: RNA is collected at 24–48 h, proteins at 48–72 h, and functional validation is conducted at 24–48 h. The lentiviral vectors were packaged utilizing three plasmids and cultured in 293T cells (ATCC, USA). The plasmid used for E2F2 overexpression ($E2F2^{OE}$) was pcSLenti-EF1-EGFP-P2A-Puro-CMV-E2F2-3xFLAG-WPRE, and the corresponding negative control plasmid (NC^{OE}) was pcSLenti-EF1-EGFP-P2A-Puro-CMV-MCS-3xFLAG-WPRE (Hanyuan Bioscience, China). Cells at 30%–40% confluency were infected with the lentivirus. Within 24 h, the medium was replaced with a fresh culture medium, and after 72 h, it was replaced with a screening medium containing 5 μg/ml puromycin. After one week of drug screening, cells were ready for subsequent detection experiments.

CCK-8 assay

Cells were seeded into 96-well plates at a density of 5×10^3 cells per well, and the assay was conducted at four distinct time intervals: 0, 24, 48, and 72 h. At each time, 10 μl of Cell Counting Kit-8 (CCK-8) (Solarbio, China) solution was introduced into every well of the experimental and control groups. For drug concentration screening, the culture medium containing the specified drug concentration was refreshed every 24 h to maintain its efficacy. Following the addition of CCK-8, the plates were incubated in a cell culture incubator for 2 h, and the optical density at 450 nm was measured utilizing a microplate reader (Tecan, Switzerland).

Wound healing assay

When the cell confluency exceeded 90%, a straight-line scratch was created across the cell monolayer in each well utilizing a 100 μl pipette tip. The wells were rinsed with PBS to remove any dislodged cells, and the medium was replaced with a complete medium containing 1% FBS. The width of the scratch was photographed and recorded under an inverted microscope at 0 h and 24 h post-scratch. The cell migration rate (%) was calculated utilizing the following formula: Cell migration rate (%) = [(Scratch width at 0 h − Scratch width at 24 h) / Scratch width at 0 h] × 100.

Transwell assay

For migration assays, Transwell chambers without Matrigel were used, while invasion assays utilized chambers coated with Matrigel. Cells were harvested with trypsin (Gibco, USA), counted, and then resuspended in a serum-free medium at a density of 1×10^6 cells/ml. Then, 200 μl of the cell suspension was transferred into the upper chamber of each Transwell, and 500 μl of

Table 2 siRNA Sequences

siRNA Name	Sense Strand(5′→3′)	Antisense Strand (5′→3′)
NC^{SI}	UUCUCCGAACGUGUCACGUTT	ACGUGACACGUUCGGAGAATT
$E2F2^{SI1}$	GCUACUGCUACCUACUACACATT	UGUGUAGUAGGUAGCAGUAGCTT
$E2F2^{SI2}$	GCGAUCUCUUCGACUCCUACGTT	CGUAGGAGUCGAAGAGAUCGCTT
$E2F2^{SI3}$	AGGACAACCUGCAGAUAUAUCTT	GAUAUAUCUGCAGGUUGUCCUTT

complete medium with 20% FBS was placed in the lower chamber. The cells were then incubated for 48 h. After incubation, the medium was discarded, and non-migrating or non-invading cells on the upper side of the filter membrane were gently removed with a cotton swab. The chambers were subsequently washed with PBS. The cells on the lower surface of the filter membrane were fixed with 500 µl of 4% paraformaldehyde for 20 min. Following fixation, the chambers were removed, inverted, and air-dried, followed by staining with 0.1% crystal violet solution for 20 min. The membranes were subsequently rinsed twice with PBS. Finally, cells that had migrated or invaded the lower membrane side were observed, imaged, and counted under an inverted microscope.

Cell apoptosis assay

Cells were treated with EDTA-free trypsin and collected at a concentration of 5×10^5 cells. The cells were resuspended in 500 µl of Binding Buffer to create a uniform single-cell suspension. Next, 5 µl of Annexin V-FITC and 5 µl of Propidium Iodide were added, and the mixture was incubated in the dark at RT for 5–10 min. The apoptosis rate was determined utilizing a flow cytometer (BD Biosciences, USA) and calculated as the sum of Q2 and Q3.

Cell cycle assay

Cells were rinsed with PBS, collected, and adjusted to a cell concentration of 1×10^6 cells/ml. After centrifugation, the cell pellet was resuspended in 500 µl of 70% cold ethanol and fixed at 4 °C overnight. Before staining, cells were rinsed with PBS to remove the fixative. A staining solution containing RNase A and Propidium Iodide in a 1:9 ratio was introduced into the cells, and cells were incubated in the dark at RT for 30–60 min. The cell cycle analysis was conducted utilizing a flow cytometer.

RNA quality analysis, amplification, and sequencing

RNA sample purity was examined using 1% agarose gel electrophoresis, while RNA concentration was measured with a Qubit® 2.0 Fluorometer (Life Technologies, USA). RNA integrity was determined utilizing the Agilent 2100 RNA Nano 6000 Assay Kit (Agilent Technologies, USA). After confirming RNA quality, mRNA was isolated utilizing magnetic beads coated with Oligo(dT) that bind specifically to the poly-A tails of mRNA. The enriched mRNA was then fragmented into short segments and utilized as templates for synthesizing first-strand cDNA with random hexamer primers. To synthesize the second strand of cDNA, buffer, dNTPs, and DNA polymerase I were added, followed by purification. The purified double-stranded cDNA underwent end repair, the addition of an A-tail, and ligation with sequencing adapters. PCR amplification was carried out to construct the cDNA library. Cluster generation was executed on a cBot utilizing the TruSeq PE Cluster Kit v3-cBot-HS, followed by paired-end sequencing (PE150) on the Illumina sequencing platform.

Bioinformatics analysis

Read-count data generated during gene expression analysis were used to identify differentially expressed genes (DEGs). Differential expression was initially analyzed separately for experimental and control groups using the edgeR package in R. DESeq was then used to assess overall DEGs between the groups. Genes with a p-value below 0.05 and a fold change (FC) of 2 or greater were identified as DEGs. Expression levels of DEGs across all samples were compiled, and bidirectional clustering of genes and samples was performed using the appropriate R package.

Methylation-specific PCR (MSP)

Cellular DNA was fully extracted, and concentration and quality were confirmed. The DNA was then modified and purified using a bisulfite conversion and purification kit (EZBioscience, USA). Methylation-specific PCR was performed with an MSP kit (Tiangen Biotech, China). The 20 µl reaction system included 2 µl of DNA template, 1 µl each of forward and reverse primers, 1.6 µl of dNTPs (2.5 mM), 0.4 µl of MSP DNA Polymerase (2.5 U), 2 µl of 10×MSP PCR Buffer, and 12.6 µl of ddH_2O. PCR conditions were as follows: initial denaturation at 95 °C for 5 min; 35 cycles of denaturation at 94 °C for 20 s, annealing at 60 °C for 30 s, and extension at 72 °C for 20 s, with a final extension at 72 °C for 5 min. Following PCR, 10 µl of the product was subjected to agarose gel electrophoresis, and results were captured and analyzed using a chemiluminescent gel imaging system (Epizyme, China). The E2F2 promoter sequences were obtained from the genome database, and high-quality primer sequences were generated using Meth Primer software. The sequences of the primers utilized are provided in Table 3.

Statistical analysis

Statistical analyses were carried out utilizing GraphPad Prism 10.1.2. A t-test was utilized to assess the differences between the two experimental groups. For comparisons involving more than two groups, one-way or two-way analysis of variance (ANOVA) was applied. Correlation analyses were performed using Pearson's correlation coefficient for normally distributed continuous data and Spearman's rank correlation coefficient for non-normally distributed continuous data or ordinal data. $P<0.05$ was considered statistically significant.All experiments were performed three times independently. Data

Table 3 Methylation-Specific PCR Primer Sequences

Gene Name	Forward(5′→3′)	Reverse(5′→3′)
Methylated E2F2	GTATTTAGGTGTTGTGTGGTTTAGC	ACCATAATCACTAAAAATCCTCGTA
Unmethylated E2F2	ATTTAGGTGTTGTGTGGTTTAGTGT	CCATAATCACTAAAAATCCTCATA

were presented as the mean ± SD. (*,$P<0.05$; **, $P<0.01$; ***, $P<0.001$).

Results

Expression of E2F2

E2F2 serves as a crucial transcription factor, playing a significant role in cell cycle regulation, proliferation, and apoptosis. The regulatory mechanisms governing its expression and activity are highly complex, involving multiple layers including post-transcriptional regulation, modulation by various signaling pathways, as well as genetic variations and epigenetic modifications of the gene itself. Consequently, the expression levels of E2F2 can vary greatly among different types of tumors.

TIMER 2.0 analysis revealed that E2F2 is downregulated in certain malignant tumors. Notably, the mRNA levels of E2F2 were markedly reduced in cancerous tissues, such as colon adenocarcinoma (COAD) ($P<0.01$) and rectal adenocarcinoma (READ) ($P<0.05$) versus adjacent normal tissues(Fig. 1a). MG cells appeared round, oval, or polygonal, maintaining a normal nuclear-to-cytoplasmic ratio (Fig. 1b). In contrast, MGC cells exhibited a round, oval, or polygonal shape with closely packed intercellular arrangements, forming cohesive sheets. These cells displayed well-defined contours, large nuclei, scant cytoplasm, a high nuclear-to-cytoplasmic ratio, and marked atypia (Fig. 1c). The findings demonstrated that both mRNA and protein levels of E2F2 were lower in MGC cells compared to MG cells (Fig. 1d).

E2F2 levels in tissue microarrays and its relationship with P21 and P27

The tissue microarray analysis indicated that E2F2 levels were lower in meibomian gland carcinoma than in normal meibomian gland tissue. Despite the immunohistochemical staining in tissue microarrays revealing that the high expression level of E2F2 is similar to the staining intensity observed in normal meibomian gland adenocarcinoma tissues, this does not pose a contradiction. In fact, the high expression of E2F2 reflects individual variations among a minority of samples within the tissue microarrays, and notably, this high expression is often accompanied by a relatively lower malignancy degree in patients. Therefore, this finding further supports the notion that E2F2 has a tumor-suppressing role in meibomian gland adenocarcinoma. The differences in E2F2 expression levels provide valuable clues and research directions for us to delve deeper into its functional mechanisms in meibomian gland adenocarcinoma. Specifically, immunohistochemical staining results have revealed a negative correlation trend between E2F2 and Ki-67 expression, as well as a positive correlation trend between E2F2 and P21, P27 expression. However, it is important to note that due to the relatively limited number of samples collected in this study, the regression coefficients obtained are below 0.5. These trend-based conclusions can be further consolidated and validated through functional verification at the cellular level. (Fig. 2).

Successful Modulation of E2F2 expression levels by siRNA transfection or lentiviral infection

Since the $E2F2^{SI}$ group of small interfering RNAs (siRNAs) lacked fluorescent labeling, transfection efficiency was observed indirectly by comparing fluorescence intensity with the NC^{SI} group, a fluorescently labeled control. Fluorescence microscopy showed detectable fluorescent signals in the NC^{SI}, NC^{OE}, and $E2F2^{OE}$ groups of MGC cells (Supplementary Information: Figure S1a-c). RT-qPCR and Western blot analyses verified a decrease in both mRNA and protein levels of E2F2 in the $E2F2^{SI}$ group versus the NC group. The most effective siRNA, $E2F2^{SI3}$, was selected for further experiments and referred to as $E2F2^{SI}$(Figs. 3a、b). Conversely, E2F2 expression was increased in the $E2F2^{OE}$ group (Figs. 3c、d).

Effects of E2F2 on proliferation, migration, invasion, and epithelial-mesenchymal transition (EMT) in MGC cells

To systematically evaluate the specific role of E2F2 in the biological behavior of meibomian gland carcinoma, we designed and conducted a series of functional validation experiments. Knockdown of E2F2 ($E2F2^{SI}$ group) promoted MGC cell proliferation versus the NC group, while overexpression of E2F2 ($E2F2^{OE}$ group) inhibited the proliferation of MGC cells (Fig. 4a, b). The migratory and invasive capacities of MGC cells were enhanced in the $E2F2^{SI}$ group but decreased in the $E2F2^{OE}$ group versus the NC group (Fig. 4c, d, e). Furthermore, a significant downregulation of E-Cadherin mRNA and protein

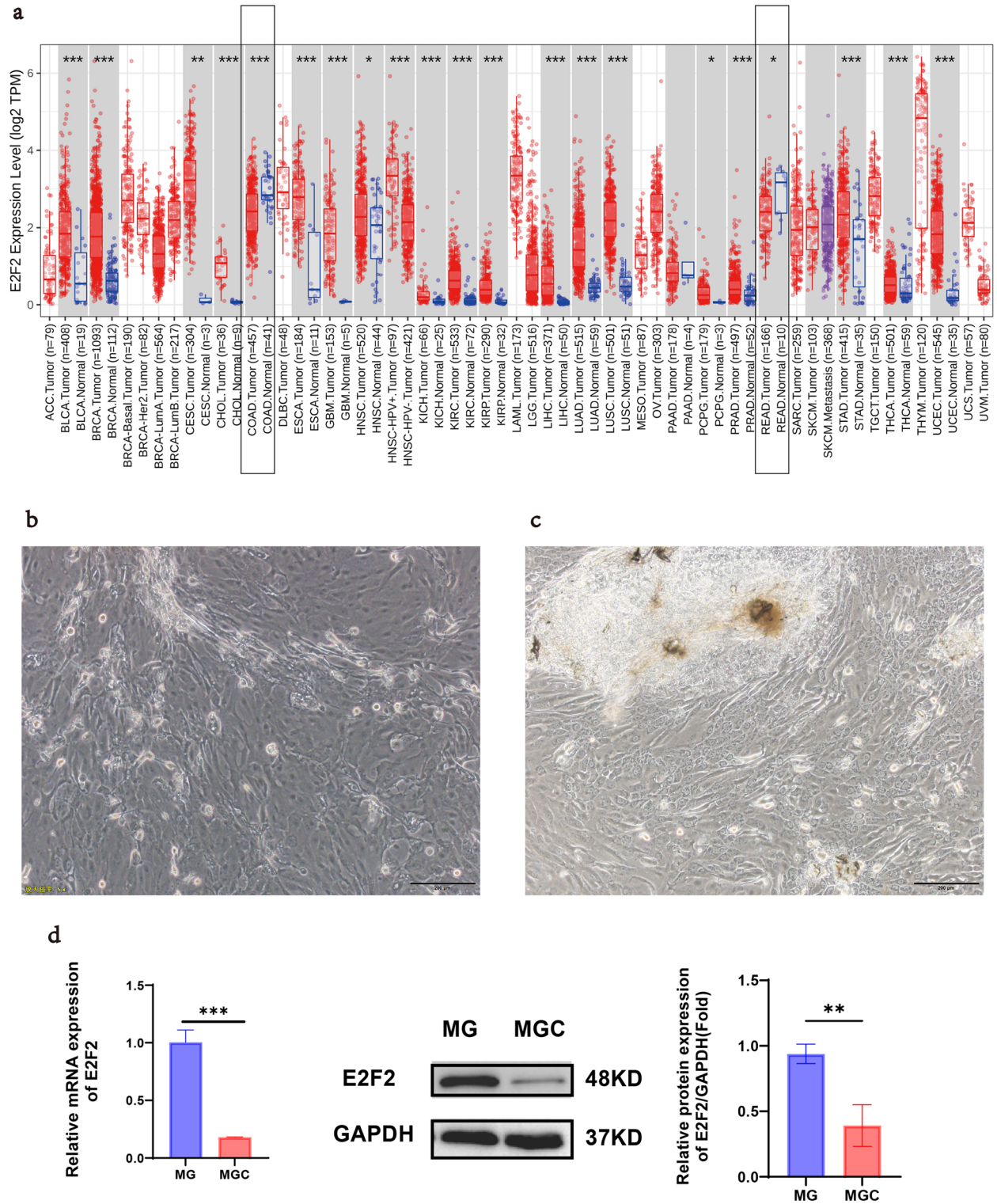

Fig. 1 Expression of E2F2. **a** Differential expression of E2F2 between various tumors or specific tumor subtypes and adjacent normal tissues. **b** MG cells exhibit an oval, short spindle or polygonal shape, with a normal nuclear-to-cytoplasmic ratio (×40). **c** MGC cells display an oval or round shape with significant atypia and tight intercellular connections (×40). **d** Differential E2F2 mRNA and protein expression between primary MG and MGC cells. *$P < 0.05$; **$P < 0.01$; ***$P < 0.001$

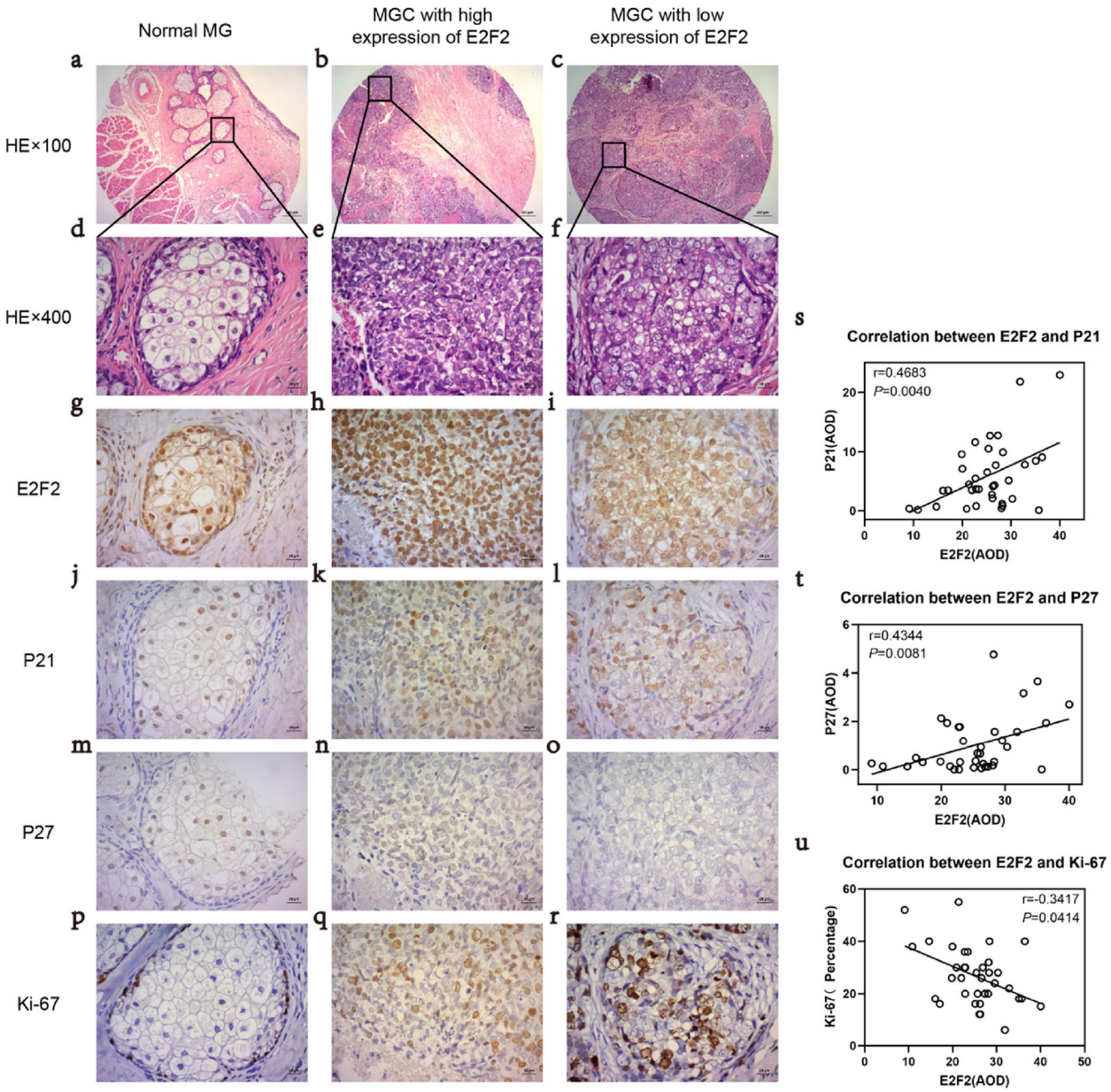

Fig. 2 Tissue Microarray. **a** Normal meibomian gland with lobular gland arrangement. **b**, **c** HE staining of two MGC cases showed a loss of normal lobular structure and infiltrative growth patterns. **d** Magnified view of the boxed area in (**a**) highlighting the peripheral edge of a normal meibomian gland lobule with cuboidal, basophilic basal cells and a center of multilayered vacuolated cells with lipid-rich cytoplasm. **e**, **f** Magnified views of the boxed areas in (**b**) and (**c**) show carcinoma cells with a low nucleus-to-cytoplasm ratio, some with retained lipids in the cytoplasm, and frequent mitotic figures. **g** Uniform E2F2 expression in the nuclei of normal meibomian gland cells. **h** High E2F2 expression in a case of MGC. **i** Compared to (**h**), another case with low E2F2 expression shows weaker staining. **j**, **m** Nuclear expression of P21 and P27 in vacuolated cells of normal meibomian glands. **k**, **n** Intense P21 and P27 staining in MGC cases with low E2F2 expression. **l**, **o** Weak P21 and P27 staining in MGC cases with high E2F2 expression. **p** Ki-67 expression in basal cells of normal meibomian glands. **q** Reduced Ki-67 expression in cases with high E2F2 expression. **r** Increased Ki-67 expression in cases with low E2F2 expression. **s** Positive correlation between E2F2 and P21 expression. (t) Positive correlation between E2F2 and P27 expression. **u** Negative correlation between E2F2 and Ki-67 expression

levels was observed in the $E2F2^{SI}$ group, while these levels were upregulated in the $E2F2^{OE}$ group(Fig. 4f,g).

Impact of E2F2 on apoptosis and cell cycle progression in MGC cells

Flow cytometry revealed a reduced apoptosis rate in MGC cells in the $E2F2^{SI}$ group versus the NC group

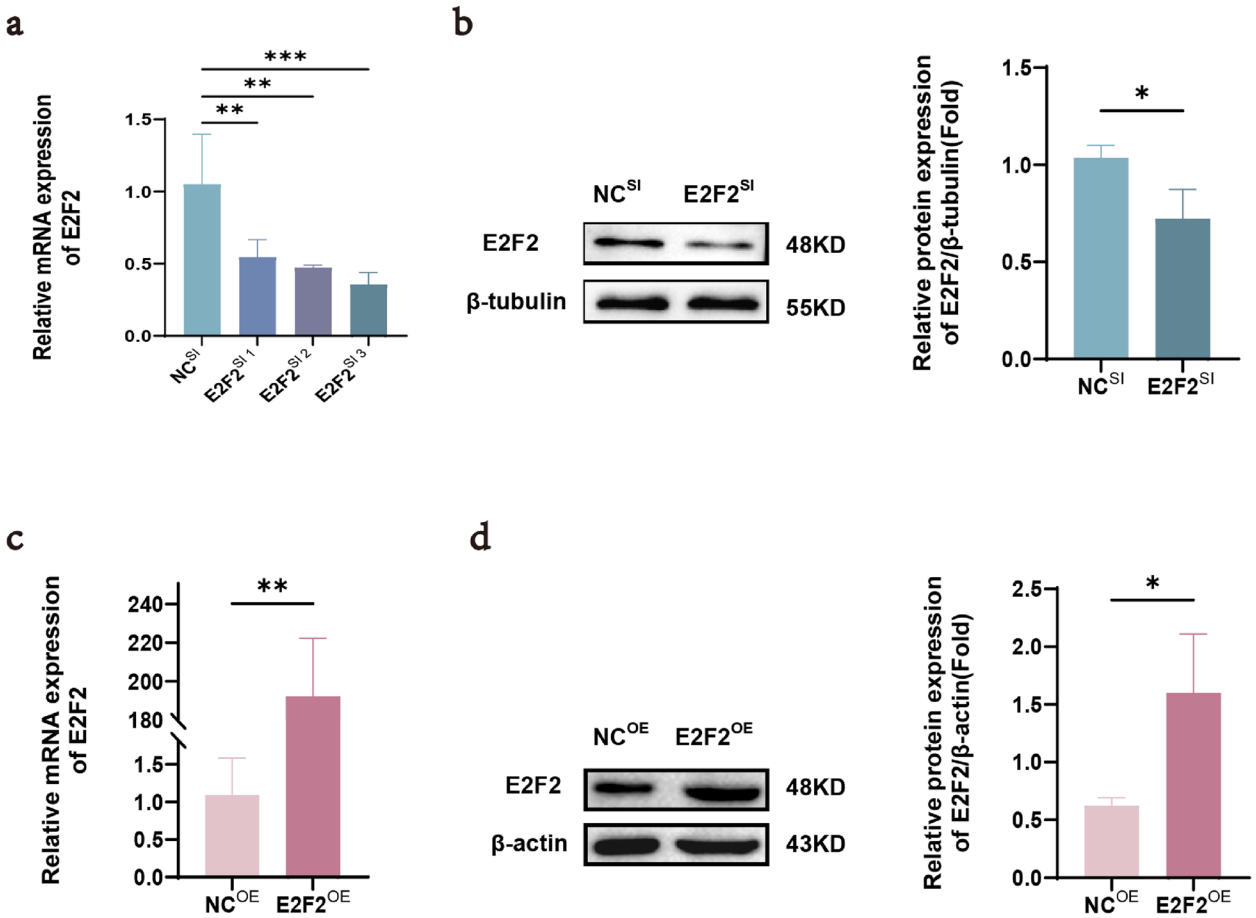

Fig. 3 Knockdown and Overexpression of E2F2. **a**, **b** qRT-PCR and Western blot analysis validating successful E2F2 knockdown in MGC cells using siRNA. **c**, **d** qRT-PCR and Western blot analysis validating successful E2F2 overexpression in MGC cells using lentiviral vectors.*$P < 0.05$; **$P < 0.01$; ***$P < 0.001$

(Fig. 5a). The $E2F2^{SI}$ group markedly decreased mRNA and protein expression levels of the apoptosis-related markers Bax and Caspase-3 (Fig. 5b, c). Additionally, there was a significant decrease in the percentage of MGC cells in the G0/G1 stage and an increase in the S stage, with no significant changes detected in the G2 stage (Fig. 5d). The mRNA expression levels of cell cycle regulators P16, P21, and P27 were significantly decreased, whereas the mRNA expression level of CDK4 was notably elevated in the $E2F2^{SI}$ group (Fig. 5e). In contrast, the $E2F2^{OE}$ group exhibited opposite effects.

Bioinformatics analysis of differentially expressed genes in MGC cells treated with 5-aza-2-dc identified by RNA-Seq

The optical density (OD) values of the experimental groups treated with different concentrations of 5-aza-2-dc were lower than those of the control group, suggesting that reducing DNA methylation levels with 5-aza-2-dc significantly reduces the proliferative capacity of MGC cells. Based on safety and concentration-dependent effects, the minimum effective dose of 10 μmol/L, which resulted in a high tumor cell inhibition rate, was selected as the optimal concentration for subsequent experiments (Fig. 6a). MGC cells were treated with 10 μmol/L of 5-aza-2-dc (treatment group), and their gene transcription levels were compared with those of untreated MGC cells (control group). The volcano plot identified 87 DEGs, with 72 upregulated and 15 downregulated, showing that the number of upregulated mRNAs significantly exceeded the downregulated ones (Fig. 6b, c). The dendrogram located on the left side of the figure represents the hierarchical clustering analysis of gene expression patterns, clearly illustrating the similarities among genes. Shorter branches on the dendrogram signify that the genes display more similar expression profiles across different samples. The line positioned at the top of the figure signifies the clustering of samples. Furthermore, the clustering heatmap confirms a certain degree of consistency in the expression patterns of differentially expressed

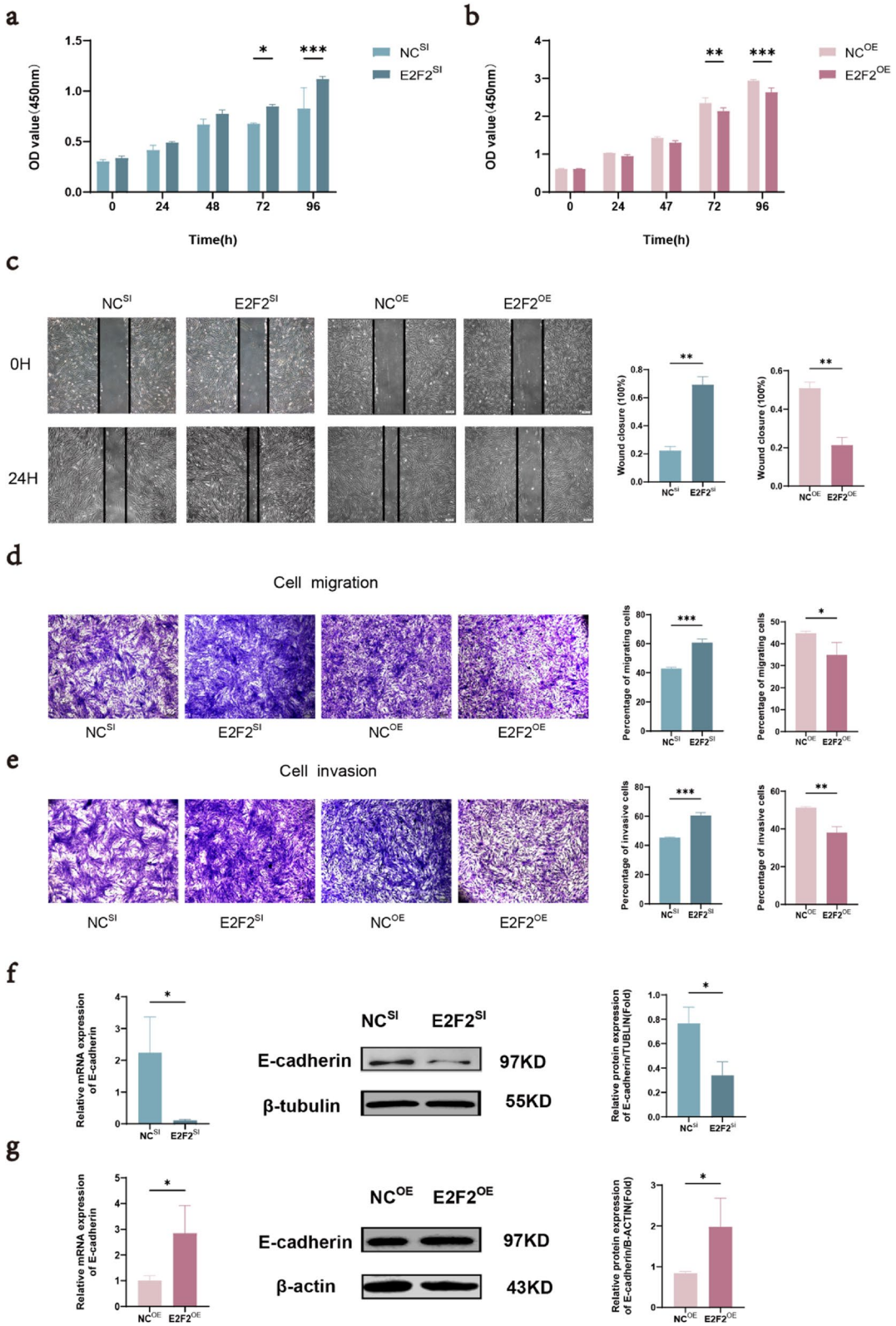

Fig. 4 Effects of E2F2 on Proliferation, Migration, Invasion, and Epithelial-Mesenchymal Transition in Primary MGC Cells. **a**, **b** CCK-8 assay validating the effect of E2F2 regulation on cell proliferation. **c**, **d** Wound healing and Transwell assays validate the effect of E2F2 regulation on cell migration. **e** Transwell assay indicating the effect of E2F2 regulation on the invasion of MGC cells. **f**, **g** qRT-PCR and Western blot analyses assessing the effect of E2F2 regulation on E-cadherin expression.*$P < 0.05$; **$P < 0.01$; ***$P < 0.001$

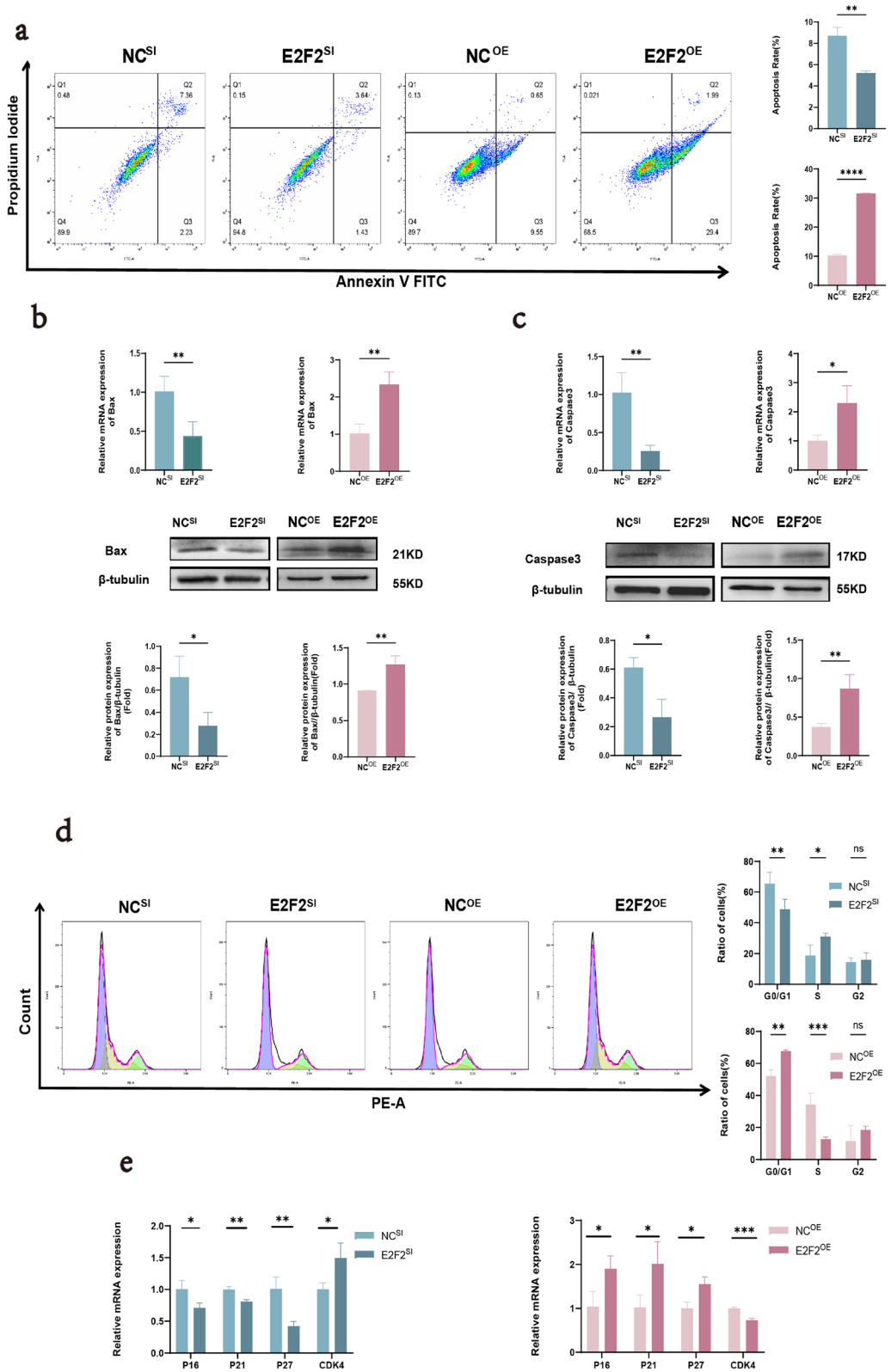

Fig. 5 Effects of E2F2 on Apoptosis and Cell Cycle in MGC Cells. **a** Flow cytometry analysis of cell apoptosis, with quantification based on the apoptosis rate. **b**, **c** RT-qPCR and Western blot analyses of the expression of apoptosis-related proteins Bax and Caspase-3. **d** Flow cytometry analysis of the distribution of cells across different phases of the cell cycle. **e** RT-qPCR analysis of the expression levels of cell cycle-related genes P16, P21, P27, and CDK4.*$P < 0.05$; **$P < 0.01$; ***$P < 0.001$

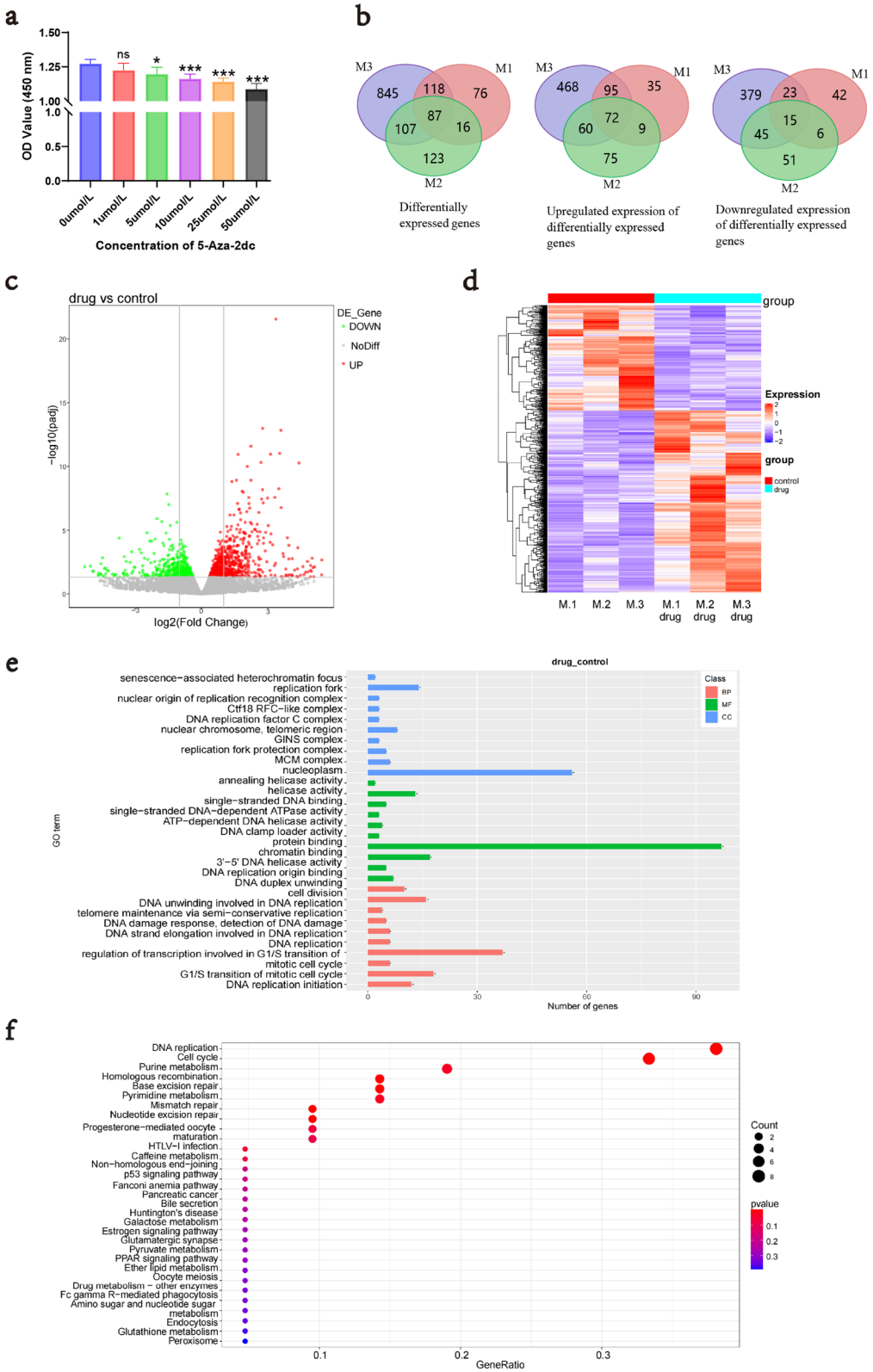

Fig. 6 Enrichment Analysis of Differentially Expressed Genes (DEGs) and RNA-Seq Data. **a** OD values of MGC cells treated with different concentrations of 5-aza-2-dc for 72 h. **b** Venn diagram showing the overlap of DEGs. **c** Volcano plot of DEGs: green dots represent downregulated genes, and red dots represent upregulated genes. **d** Hierarchical clustering heatmap of DEGs. **e** GO enrichment analysis of DEGs. **f** KEGG pathway enrichment analysis of DEGs

genes across various samples (Fig. 6d). Among the top ten upregulated DEGs ranked by fold change (FC) and P-value, the genes identified as potentially downregulated by DNA methylation included ESM1, OPCML, E2F2, FAM111B, MCM10, CLSPN, MT2A, CDC45, CDC6, and EXO1, as detailed in Table 4.

GO enrichment analysis showed that the DEGs were primarily involved in biological processes (BP) related to DNA replication, cell mitosis, DNA duplex unwinding, homologous recombination repair of double-strand breaks, and DNA extension during replication. In terms of cellular components (CC), these genes were mainly located in the nucleoplasm, MCM complex, replication fork protection complex, GINS complex, nuclear chromosome telomeric region, and Ctf18 RFC-like complex. For molecular functions (MF), significant roles included protein binding, ATP binding, chromatin binding, helicase activity, histone binding, and single-stranded DNA binding (Fig. 6e). KEGG pathway enrichment analysis further highlighted associations of DEGs with critical pathways such as DNA replication, cell cycle, purine metabolism, homologous recombination, base excision repair, and pyrimidine metabolism (Fig. 6f).

5-aza-2-dc Reduces E2F2 Methylation Levels in MGC Cells and Affects Cell Migration and Invasion

RT-qPCR results indicated that treatment with 10 μmol/L 5-aza-2-dc for 72 h led to increased mRNA expression levels of ESM1, OPCML, E2F2, FAM111B, MCM10, CLSPN, MT2A, CDC45, CDC6, and EXO1 in MGC cells compared to the control group, consistent with RNA-Seq findings (Fig. 7a). Meanwhile, we validated the expression of these 10 differentially expressed genes in normal meibomian glands and meibomian gland carcinomas, respectively (Supplementary Information: Figure S2). MSP analysis showed that the methylated E2F2 band was reduced, while the unmethylated band was intensified in the 5-aza-2-dc-treated group, indicating decreased E2F2 methylation levels in MGC cells (Fig. 7b). The wound healing and Transwell assays revealed a notable decrease in the migration and invasion capabilities of MGC cells following treatment with 5-aza-2-dc (Fig. 7c, d). These findings suggest that inhibiting methylation levels in MGC cells have effects similar to those observed with E2F2 overexpression on the biological behavior of MGC cells.

Discussion

Meibomian gland carcinoma (MGC) is a malignant epithelial tumor of the eyelid with a rising global incidence [20, 21]. While surgical treatment can achieve complete tumor removal, the high risk of postoperative recurrence, local invasion, and distant metastasis remains a critical challenge affecting patient prognosis. Therefore, exploring effective molecular-targeted therapies and identifying novel biomarkers and molecular targets to inhibit MGC progression is essential.

This study focuses on E2F2, a transcription factor of the E2F family known for its pivotal role in controlling the cell cycle and DNA synthesis in malignant tumors. E2F2 is critical in the progression of different types of cancers [22–25]. Studies have shown that E2F2 may impact cell proliferation, angiogenesis, and invasion in different tumor cell types [26, 27]. For instance, in colorectal cancer (CRC), downregulation of E2F2 is associated with tumor N and M stages, as well as the overall pathological stage [28]. Li et al. demonstrated the tumor-suppressive function of E2F2 in CRC by inhibiting survivin expression and regulating gene expression [29]. Mitlianga et al. reported that the co-expression of E2F2 and p53 improves the anticancer properties of p53 in glioblastoma cells [30]. Despite these insights, the specific role and molecular mechanisms of E2F2 in MGC remain unclear.

Table 4 Expression of Major Upregulated Genes Identified by RNA Sequencing

Name	log2FC	P value	Trend	Description
ESM1	4.395837277	1.66E-07	UP	endothelial cell specific molecule 1
OPCML	3.938892985	0.038909393	UP	opioid binding protein/cell adhesion molecules like
E2F2	3.879287994	0.014805477	UP	e2f transcription factor 2
FAM111B	3.581304033	1.39E-09	UP	family with sequence similarity 111 member B
MCM10	3.52899728	4.55E-08	UP	minichromosome maintenance 10 replication initiation factor
CLSPN	3.48946466	1.13E-05	UP	claspin
MT2A	3.354432718	7.74E-18	UP	metallothionein 2A
CDC45	3.310001731	3.92E-05	UP	cell division cycle 45
CDC6	3.111532265	1.10E-11	UP	cell division cycle 6
EXO1	2.680445001	4.93E-11	UP	exonuclease 1

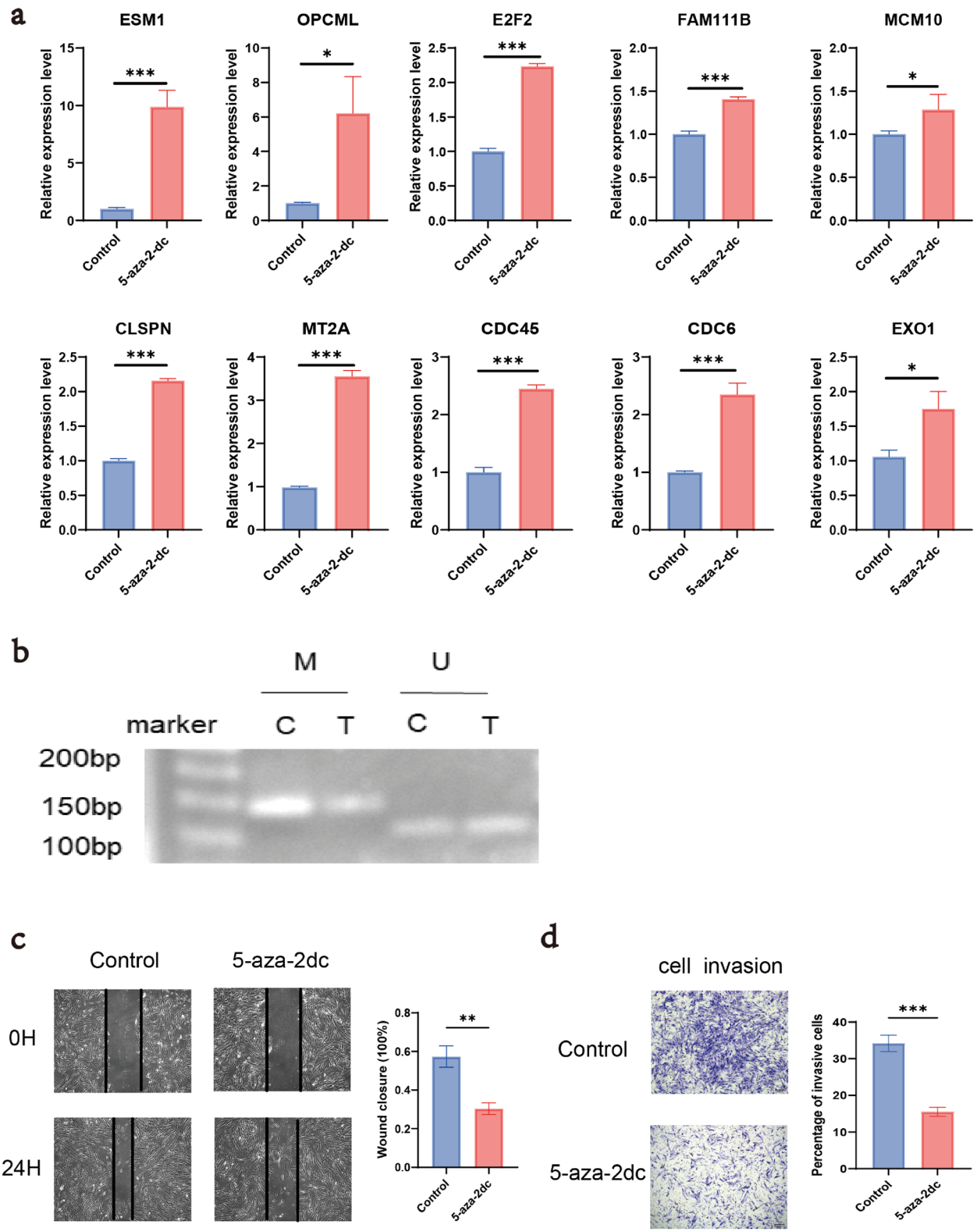

Fig. 7 Effects of 5-aza-2-dc on MGC Cells. **a** Changes in mRNA expression levels of the top ten genes in MGC cells following 5-aza-2-dc treatment. **b** Reduction in E2F2 methylation levels and increase in unmethylated levels in MGC cells after 5-aza-2-dc treatment (M: methylated band; U: unmethylated band; C: control group; T: 5-aza-2-dc treatment group). **c**, **d** Effects of 5-aza-2-dc on the migration and invasion of MGC cells. $^{*}P < 0.05$; $^{**}P < 0.01$; $^{***}P < 0.001$

In our study, tissue microarray analysis showed that E2F2 expression is reduced in MGC tissues. Its expression is negatively correlated with the proliferation marker Ki-67 while positively correlated with the cell cycle regulators P21 and P27. These findings suggest that E2F2 potentially suppresses the growth and invasion of MGC cells through cell cycle regulation. Functional assays further demonstrated that overexpression of E2F2 significantly inhibited MGC cell growth, migration, and invasion while promoting apoptosis and inducing G1 phase cell cycle arrest, which decreased the S-phase cell population. These findings support the hypothesis that E2F2 can slow abnormal cell proliferation by modulating the cell cycle. Additionally, tumor invasion and metastasis are primarily driven by EMT, characterized by the downregulation of cell adhesion molecules like E-cadherin [31]. In our study, inhibition of E2F2 expression led to EMT-like changes in MGC cells, underscoring E2F2's role in suppressing tumor invasion.

Epigenetic mechanisms such as DNA methylation, histone modifications, and non-coding RNA regulation play a key role in tumor development and progression [32, 33]. Methylation of tumor suppressor genes and cell cycle regulators frequently occurs in malignancies, leading to gene silencing or cell cycle disruption [34]. Studies have shown that the demethylating agent 5-aza-2-dc can decrease methylation in targeted regions and restore gene expression [35]. Previous studies have demonstrated that 5-aza-2-dc significantly inhibits the proliferation of cells in cancers such as lung and ovarian cancer. However, research on its effects on MGC remains limited [36–39]. In MGC, DNA methylation may promote tumor progression by silencing tumor suppressor genes like E2F2. To test this hypothesis, we employed 5-aza-2-dc as a demethylating agent to examine its impact on E2F2 expression in MGC cells. The findings demonstrated that 5-aza-2-dc decreased the methylation levels of E2F2, thereby restoring its expression in MGC cells. RNA sequencing analysis further revealed that genes associated with DNA replication and cell cycle regulation were significantly upregulated in MGC cells following 5-aza-2-dc treatment, aligning with the typical effects of demethylation. This finding supports the hypothesis that E2F2 undergoes epigenetic alterations in MGC. Moreover, inhibiting gene methylation in MGC cells reduced their proliferation, migration, and invasion, mirroring the effects observed with E2F2 overexpression.

Conclusions

In summary, our study is the first to demonstrate that E2F2 is significantly underexpressed in MGC and that E2F2 knockdown promotes the growth, migration, invasion, and EMT of MGC cells, affecting apoptosis and modulating various stages of the cell cycle. Additionally, we hypothesize that the downregulation of E2F2 in MGC may result from epigenetic silencing and that demethylation treatment can restore its expression, thereby inhibiting the malignant behaviors of the tumor. These findings indicate that E2F2 may be a critical therapeutic target for MGC, offering new theoretical insights for clinical interventions. Future research should further investigate the clinical potential of E2F2 in MGC therapy, particularly in the context of combining molecular targeted therapies with epigenetic regulation.

Abbreviations

MGC	Meibomian Gland Carcinoma
MG	Meibomian Gland
E2F2	E2F transcription factor 2
EMT	Epithelial-Mesenchymal Transition
5-aza-2-dc	5-Aza-2′-deoxycytidine
TIMER2.0	Tumor Immune Estimation Resource, version 2
OD	Optical Density
HE	Hematoxylin and Eosin
IHC	Immunohistochemical
DEGs	Differentially Expressed Genes
MSP	Methylation-Specific PCR
COAD	Colon Adenocarcinoma
READ	Rectal Adenocarcinoma
FC	Fold Change
BP	Biological Processes
CC	Cellular Components
MF	Molecular Functions

Supplementary Information

The online version contains supplementary material available at https://doi.org/10.1186/s12885-025-13833-6.

Supplementary Material 1

Supplementary Material 2

Acknowledgements

We would like to thank our mentor and all the teachers for their guidance and strong support during the research and writing process of this paper.

Authors' contributions

W.W: Data collection/analysis, manuscript writing, study design, statistical analysis; H.T.W: Data collection/analysis, data curation; X.L: Study design, data curation; F.X, Q.T, C.L.Z and J.Q.L: Data collection/analysis; L.M.Z.: Research supervision, funding support; T.T.L: Manuscript revision, study design, manuscript review, funding support. All authors have read and agreed to the published version of the manuscript.

Funding

This work was supported by the Open Project of Tianjin Key Laboratory of Retinal Functions and Diseases (2021tjswmm001), Tianjin Health Science and Technology Project (TJWJ2022MS012) and Tianjin Key Medical Discipline (Specialty) Construction Project (TJYXZDXK-037A).

Data availability

The datasets used and/or analyzed during the current study are available from the corresponding author upon reasonable request. And the data reported in this paper have been deposited in the OMIX, China National Center for Bioinformation / Beijing Institute of Genomics, Chinese Academy of Sciences (https://ngdc.cncb.ac.cn/omix/preview/uTT6z5xb:accessionno.OMIX007915).

Declarations

Ethics approval and consent to participate
All patients provided informed consent, and the study was approved by the Ethics Committee of Tianjin Medical University Eye Hospital with approval number [2018KY(L)-43].

Consent for publication
Not applicable.

Competing interests
The authors declare no competing interests.

Author details
[1]Tianjin Key Laboratory of Retinal Functions and Diseases, Tianjin Branch of National Clinical Research Center for Ocular Disease, Eye Institute and School of Optometry, Tianjin Medical University Eye Hospital, Tianjin 300384, China. [2]Chengdu Women'S and Children'S Central Hospital, School of Medicine,, University of Electronic Science and Technology of China, Chengdu 611731, China. [3]Department of Ophthalmology, West China Hospital, Sichuan University, Chengdu 610041, Sichuan, China. [4]Tianjin Eye Hospital Optometric Center, Tianjin 300020, China. [5]Clinical College of Ophthalmology, Tianjin Medical University, Tianjin Key Laboratory of Ophthalmology and Visual Science, Tianjin Eye Institute, Tianjin Eye Hospital, Tianjin 300020, China.

Received: 11 November 2024 Accepted: 27 February 2025
Published online: 16 May 2025

References

1. Wang L, Shan Y, Dai X, You N, Shao J, Pan X, Gao T, Ye J. Clinicopathological analysis of 5146 eyelid tumours and tumour-like lesions in an eye centre in South China, 2000–2018: a retrospective cohort study. BMJ Open. 2021;11(1):e041854.
2. Esmaeli B, Nasser QJ, Cruz H, Fellman M, Warneke CL, Ivan D. American Joint Committee on Cancer T category for eyelid sebaceous carcinoma correlates with nodal metastasis and survival. Ophthalmology. 2012;119(5):1078–82.
3. Sa HS, Rubin ML, Xu S, Ning J, Tetzlaff M, Sagiv O, Kandl TJ, Esmaeli B. Prognostic factors for local recurrence, metastasis and survival for sebaceous carcinoma of the eyelid: observations in 100 patients. Br J Ophthalmol. 2019;103(7):980–4.
4. Muqit MM, Foot B, Walters SJ, Mudhar HS, Roberts F, Rennie IG. Observational prospective cohort study of patients with newly-diagnosed ocular sebaceous carcinoma. Br J Ophthalmol. 2013;97(1):47–51.
5. Shields JA, Demirci H, Marr BP, Eagle RC Jr, Shields CL. Sebaceous carcinoma of the ocular region: a review. Surv Ophthalmol. 2005;50(2):103–22.
6. Huang R, Zhou PK. DNA damage repair: historical perspectives, mechanistic pathways and clinical translation for targeted cancer therapy. Signal Transduct Target Ther. 2021;6(1):254.
7. Perez-Herrero E, Fernandez-Medarde A. Advanced targeted therapies in cancer: Drug nanocarriers, the future of chemotherapy. Eur J Pharm Biopharm. 2015;93:52–79.
8. Sharma N, Timmers C, Trikha P, Saavedra HI, Obery A, Leone G. Control of the p53–p21CIP1 Axis by E2f1, E2f2, and E2f3 is essential for G1/S progression and cellular transformation. J Biol Chem. 2006;281(47):36124–31.
9. DeBruhl H, Wen H, Lipsick JS. The complex containing Drosophila Myb and RB/E2F2 regulates cytokinesis in a histone H2Av-dependent manner. Mol Cell Biol. 2013;33(9):1809–18.
10. Raj D, Liu T, Samadashwily G, Li F, Grossman D. Survivin repression by p53, Rb and E2F2 in normal human melanocytes. Carcinogenesis. 2008;29(1):194–201.
11. Dynlacht BD, Brook A, Dembski M, Yenush L, Dyson N. DNA-binding and trans-activation properties of Drosophila E2F and DP proteins. Proc Natl Acad Sci U S A. 1994;91(14):6359–63.
12. Reimer D, Sadr S, Wiedemair A, Concin N, Hofstetter G, Marth C, Zeimet AG. Heterogeneous cross-talk of E2F family members is crucially involved in growth modulatory effects of interferon-gamma and EGF. Cancer Biol Ther. 2006;5(7):771–6.
13. Gao Y, Qiao X, Liu Z, Zhang W. The role of E2F2 in cancer progression and its value as a therapeutic target. Front Immunol. 2024;15:1397303.
14. Campanero MR, Armstrong MI, Flemington EK. CpG methylation as a mechanism for the regulation of E2F activity. Proc Natl Acad Sci U S A. 2000;97(12):6481–6.
15. Wei D, Li A, Zhao C, Wang H, Mei C, Khan R, Zan L. Transcriptional Regulation by CpG Sites Methylation in the Core Promoter Region of the Bovine SIX1 Gene: Roles of Histone H4 and E2F2. Int J Mol Sci. 2018;19(1):213.
16. Jing X, Xu G, Gong Y, Li J. LingfengWu, Zhu W, He Y, Li Z, Pan S: A five-gene methylation signature predicts overall survival of patients with clear cell renal cell carcinoma. J Clin Lab Anal. 2021;35(12):e24031.
17. Edwards JR, Yarychkivska O, Boulard M, Bestor TH. DNA methylation and DNA methyltransferases. Epigenetics Chromatin. 2017;10:1–10.
18. Lyko F, Brown R. DNA methyltransferase inhibitors and the development of epigenetic cancer therapies. J Natl Cancer Inst. 2005;97(20):1498–506.
19. Zhang C, Zhu L, Liu X, Jiang M, Tang Q, Xu F, Lin T, He Y. Establishment of a human meibomian gland carcinoma cell model and analysis of differently expressed genes. Exp Eye Res. 2022;219:108983.
20. Dasgupta T, Wilson LD, Yu JB. A retrospective review of 1349 cases of sebaceous carcinoma. Cancer. 2009;115(1):158–65.
21. Yadlapati S, Rosa-Nieves PM, Mehta N, Merritt BG, Carrasquillo OY. Treatment of sebaceous carcinoma with Mohs micrographic surgery versus wide local excision: a systematic review. Int J Dermatol. 2024;63(10):1357–62.
22. Han Z, Mo R, Cai S, Feng Y, Tang Z, Ye J, Liu R, Cai Z, Zhu X, Deng Y, et al. Differential Expression of E2F Transcription Factors and Their Functional and Prognostic Roles in Human Prostate Cancer. Front Cell Dev Biol. 2022;10:831329.
23. Kent LN, Leone G. The broken cycle: E2F dysfunction in cancer. Nat Rev Cancer. 2019;19(6):326–38.
24. Kassab A, Gupta I, Moustafa AA. Role of E2F transcription factor in oral cancer: Recent insight and advancements. Semin Cancer Biol. 2023;92:28–41.
25. Hou B, Shu M, Liu C, Du Y, Xu C, Jiang H, Hou J, Chen X, Wang L, Wu X. Unveiling the role of UPF3B in hepatocellular carcinoma: Potential therapeutic target. Cancer Sci. 2024;115(8):2646–58.
26. Yang Y, Guo Z, Chen W, Wang X, Cao M, Han X, Zhang K, Teng B, Cao J, Wu W, et al. M2 Macrophage-Derived Exosomes Promote Angiogenesis and Growth of Pancreatic Ductal Adenocarcinoma by Targeting E2F2. Mol Ther. 2021;29(3):1226–38.
27. Chen SN, Mai ZY, Mai JN, Liang W, Dong ZX, Ju FE, Chan SH, Fang Z, Xu Y, Uziel O, et al. E2F2 modulates cell adhesion through the transcriptional regulation of PECAM1 in multiple myeloma. Br J Haematol. 2023;202(4):840–55.
28. Shang Y, Zhang Y, Liu J, Chen L, Yang X, Zhu Z, Li D, Deng Y, Zhou Z, Lu B, et al. Decreased E2F2 Expression Correlates with Poor Prognosis and Immune Infiltrates in Patients with Colorectal Cancer. J Cancer. 2022;13(2):653–68.
29. Li T, Luo W, Liu K, Lv X, Xi T. miR-31 promotes proliferation of colon cancer cells by targeting E2F2. Biotechnol Lett. 2015;37(3):523–32.
30. Mitlianga PG, Kyritsis AP, Gomez-Manzano C, Lemoine MG, Hu M, Liu TJ, Yung WK, Fueyo J. Co-expression of E2F–2 enhances the p53 anticancer effect in human glioma cells. Int J Oncol. 2001;18(2):343–7.
31. Sommariva M, Gagliano N. E-Cadherin in Pancreatic Ductal Adenocarcinoma: A Multifaceted Actor during EMT. Cells. 2020;9(4):1040.
32. Zhang L, Lu Q, Chang C. Epigenetics in Health and Disease. Adv Exp Med Biol. 2020;1253:3–55.
33. Wu SC, Zhang Y. Active DNA demethylation: many roads lead to Rome. Nat Rev Mol Cell Biol. 2010;11(9):607–20.
34. Saghafinia S, Mina M, Riggi N, Hanahan D, Ciriello G. Pan-Cancer Landscape of Aberrant DNA Methylation across Human Tumors. Cell Rep. 2018;25(4):1066-1080 e1068.
35. Christman JK. 5-Azacytidine and 5-aza-2'-deoxycytidine as inhibitors of DNA methylation: mechanistic studies and their implications for cancer therapy. Oncogene. 2002;21(35):5483–95.
36. Xiong R, Du Y, Chen S, Liu T, Ding X, Zhou J, Wang Z, Yang Q. Hypermethylation of the ADIRF promoter regulates its expression level and is

involved in NNK-induced malignant transformation of lung bronchial epithelial cells. Arch Toxicol. 2023;97(12):3243–58.
37. Ho CM, Shih DT, Hsiao CC, Huang SH, Chang SF, Cheng WF. Gene methylation of human ovarian carcinoma stromal progenitor cells promotes tumorigenesis. J Transl Med. 2015;13:367.
38. Endo Y, Uzawa K, Mochida Y, Shiiba M, Bukawa H, Yokoe H, Tanzawa H. Sarcoendoplasmic reticulum Ca(2+) ATPase type 2 downregulated in human oral squamous cell carcinoma. Int J Cancer. 2004;110(2):225–31.
39. Shi C, Yan L, Gao J, Chen S, Zhang L. Effects of ABCB1 DNA methylation in donors on tacrolimus blood concentrations in recipients following liver transplantation. Br J Clin Pharmacol. 2022;88(10):4505–14.

Publisher's Note